

ARTICLES

Observation of Translational Diffusion of Single Terrylenediimide Molecules in a Mesostructured Molecular Sieve

Christian Seebacher, Christian Hellriegel, Fred-Walter Deeg, and Christoph Bräuchle*

Department Chemie, Ludwig-Maximilians-Universität München, Butenandtstrasse 5-13 (Haus E), D-81377 München, Germany

Stephan Altmair and Peter Behrens

Institut für Anorganische Chemie, Universität Hannover, Callinstrasse 9, D-30167 Hannover, Germany

K. Müllen

*Max Planck Institute for Polymer Research, Ackermannweg 10, 55128 Mainz, Germany**Received: August 17, 2001; In Final Form: December 20, 2001*

The translational motion of single terrylenediimide (TDI) dye molecules incorporated into the organic part of a surfactant–silica mesostructure of a monolithic M41S host was observed by confocal microscopy. Only isotropic motion was found indicating that the channel-like motion lies below the optical resolution limit of the experiment. An effective diffusion constant was evaluated to be $D = 3.72 \times 10^{-2} \mu\text{m}^2 \text{s}^{-1}$. In contrast, for the TDI molecules diffusing in the pure lyotropic hexagonal phase of the same surfactant in water, a one-dimensional anisotropic diffusion with a diffusion constant of $D = 2.07 \mu\text{m}^2 \text{s}^{-1}$ was measured. The decrease in D and the occurrence of isotropic diffusion on the length scale of the optical experiment on going from the lyotropic phase to the mesostructured host are attributed to an increase in viscosity and tortuosity due to the formation of the silica walls around the template micelles in the synthesis of the M41S material. Apart from the mobile fraction, which shows normal diffusion, a stationary fraction of $\sim 10\%$ of TDI molecules is observed; however, no intermediate cases were detected.

1. Introduction

The development of various techniques for the detection, characterization, and manipulation of individual molecules has been one of the important breakthroughs in the area of optical spectroscopy within the past decade.¹ While the first investigations were limited to the organic mixed crystal pentacene/*p*-terphenyl,^{2,3} single molecule spectroscopy (SMS) could be extended to a large number of different chromophores, as well as host materials such as polymers,⁴ liquids,⁵ proteins,^{6,7} surfaces,⁸ or other systems such as semiconductor nanocrystals⁹ and defect centers in diamond.¹⁰ The fundamental advantage of SMS lies in the elimination of static heterogeneities inherent to all ensemble measurements. Furthermore, recording the fluorescence of an individual chromophore reveals dynamic phenomena that cannot be observed in bulk spectroscopy, for instance, the jumping of a molecule between the singlet and triplet manifold¹¹ or the light-induced switching of molecules between two well-defined frequencies.¹²

One of the areas of interest is presently the translational motion of chromophores and the recording of single-molecule trajectories. Schmidt et al. were the first to publish an account of single-molecule diffusion reporting on chromophore-labeled lipids in artificial membranes.¹³ There have also been investigations on the three-dimensional diffusion of single molecules in

gels¹⁴ and of freely moving molecules in solution.¹⁵ More recently, the tracking of individual viruses in a living cell labeled with a single chromophore¹⁶ and the motion of single proteins in the cell nucleus have been observed.¹⁷ SMS allows a very precise spatial localization of a single fluorophore by determining the fluorescent spot's center. The precision depends on the signal-to-noise ratio¹⁸ and is in the worst case still about an order of magnitude better than the resolution limit in the classical optical microscopy. The observation of the diffusion of individual molecules is a technique closely related to single-particle tracking (SPT).¹⁹ It delivers complementary information on a diffusing system, in particular the trajectories of the diffusing particles, which are not available from other techniques such as fluorescence correlation spectroscopy (FCS) or fluorescence photobleaching recovery (FPR). Furthermore, FCS is typically limited to diffusion faster than $0.1 \mu\text{m}^2 \text{s}^{-1}$ depending on the photobleaching behavior of the single molecule in the probed volume. In contrast to this, the diffusion of single molecules below that limit can be evaluated in analogy to SPT in a straightforward manner. This method also yields insight into the diffusion process by revealing the type of diffusion, that is, free or anomalous diffusion, and gives direct access to heterogeneities.

We have recently been able to detect single chromophores

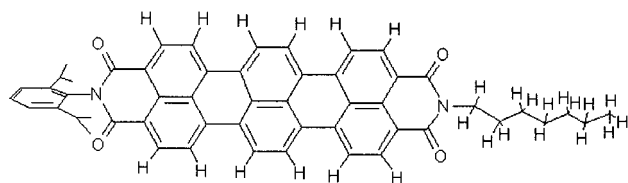


Figure 1. Chemical structure of the terrylenediimide derivative (TDI)

in mesostructured molecular sieves. By this method, we have obtained valuable spectroscopic information on this new class of host–guest materials. In this paper, we will present data on the translational diffusion of single terrylenediimide (TDI) molecules (Figure 1) located in the hydrophobic organic part of a surfactant inside the mesostructured M41S host. The surfactant was used as a template for the synthesis of the host material.²⁰ The probe molecule TDI was selected for its high photostability, which is essential for SMS investigations.²¹ M41S materials constitute promising tailor-made environments for single molecules because the interactions between the guest molecules and the host can be adjusted, for instance, by varying the pore-size and the inner surface of the pores. The inner surface can be modified chemically, ranging from charged polar groups to nonpolar organic carpets. Using this broad range of variations, one may think, in the future, of single molecules incorporated in such mesostructured materials as devices, like rotors, valves, or switches. To achieve this goal, the interactions and the degrees of freedom of single molecules in such host materials have to be characterized in detail.

There has been a longstanding interest in molecular mobility in porous materials such as zeolites.²² On one hand, diffusion is indispensable for these materials to function as ion exchangers, separation media, or catalysts. On the other hand, because of the small size and topology of the pores, molecular sieves are an ideal environment to gain a basic understanding about diffusion under geometrical constraints. Up to now, the most common techniques for the investigation of diffusion dynamics in these hosts have been pulsed-field gradient (PFG) NMR, neutron scattering, and IR microscopy.²² Standard probes used with these methods are xenon, alkanes, and benzene derivatives, which have to be present in high concentrations, so that apart from the host–guest interactions, the guest–guest interactions are always manifestly present. Diffusion constants determined by different methods on similar samples often show discrepancies of orders of magnitude.^{23,24} Novel approaches to tackle the problem of diffusion in zeolites are therefore necessary. In strong contrast to the above-mentioned methods, which probe the bulk ensemble, the tracking of individual chromophores can be performed with probe molecules in extremely low concentrations. Guest–guest interactions between the probe molecules can thus be neglected. The specific advantages and also the

limitations of the single-molecule approach to diffusion in mesostructured molecular sieves are presented in this article.

2. Experimental Section

The synthesis of mesostructured monoliths is performed according to the method of Attard et al.,²⁰ which is modified to achieve a homogeneous dye loading during the formation process. The nonionic surfactant monododecyltaethylene-glycol ether (OMO) is used as the structure-directing agent and tetramethoxysilane (TMOS) as the silica source. In a typical preparation, 0.1 mL of a 10^{-10} M solution of terrylenediimide (TDI)²⁵ in chloroform is added to 0.50 g (0.93 mmol) of OMO. The mixture is heated to a temperature of 50 °C for 12 h in an open vessel, cooled to room temperature, and then diluted in 0.50 mL of 0.01 M HCl to give a hexagonally ordered lyotropic phase. After 2 days, 1.05 mL (7.0 mmol) of TMOS is added, and the methanol generated by hydrolysis is pumped off using a gentle vacuum. The liquid product obtained is kept at room temperature for 1 day to give a viscous material. Condensation of the silica is completed by stepwise heating to 90 °C to give millimeter-sized transparent monolithic particles. In the X-ray diffraction patterns, these materials give a single peak at low diffraction angles, confirming the presence of a mesostructure as found in ref 20.

Images were recorded with a modified inverted confocal laser scanning microscope (ZEISS LSM 410). An oil immersion objective with a high numerical aperture (ZEISS 40 × 1.3 oil) was employed to achieve high spatial resolution and high light detection efficiency. The built-in HeNe laser with a wavelength of 633 nm was used for excitation. The fluorescence light was separated from the laser light using a combination of filters consisting of a dichroic mirror (Q640LP AHF Analysentechnik) and two fluorescence filters (633 nm Notch Kaiser; HQ720/150 AHF Analysentechnik). The fluorescence is detected outside the microscope with an avalanche photodiode (EG&G SPCM-AQ 141). The electronic signal-width of the photodiode is adjusted with a variable monoflop circuit and redirected to one input channel of the microscope. The electronic signal can also be routed into an autocorrelator (ALV-5000/e, ALV GmbH Langen) for fluorescence correlation spectroscopy (FCS). The samples were embedded in PMMA or in silicone to obtain a better matching of the refractive indices. The localization of the single molecule positions within a picture and the assignment of these positions to the corresponding molecules between the frames was performed manually, with the aid of automation software.

3. Results and Discussion

Figure 2 shows typical fluorescence images of a sample containing a very low concentration of TDI inside a meso-

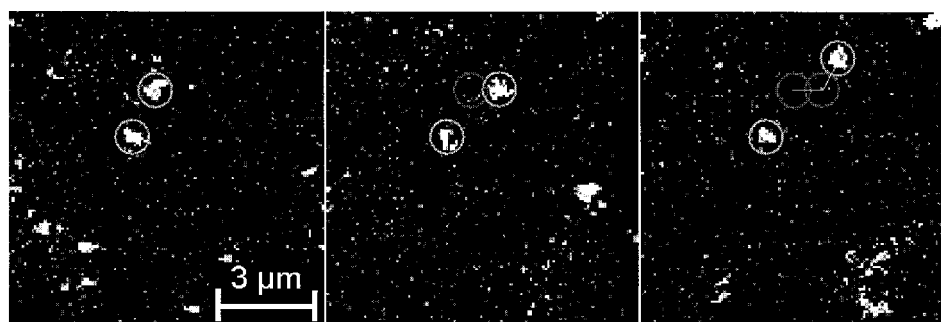


Figure 2. Diffusion of a single TDI molecule in an M41S host. A time series of three confocal fluorescence images showing emission of single TDI molecules is presented. The size of the frames depicted is $10\ \mu\text{m} \times 10\ \mu\text{m}$; time elapsed between two frames is 4 s.

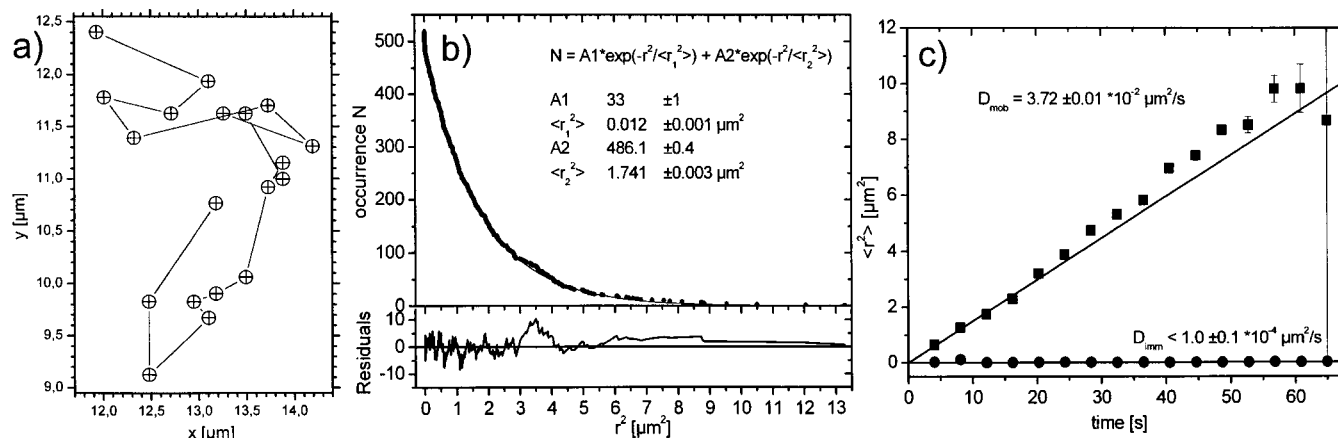


Figure 3. Characterization of diffusion by evaluation of trajectories. Panel a shows a reconstructed trajectory of a single TDI molecule in a M41S host. The time interval between two consecutive locations is 4 s. The total time span for the depicted trajectory is 72 s. A diffusion constant of $D = 0.025 \pm 0.021 \mu\text{m}^2 \text{s}^{-1}$ was evaluated from this single trajectory. Panel b shows an example for the evaluation of the mean square displacements $\langle r_i^2 \rangle$ on the basis of single-molecule trajectories for a set of frames separated by 12 s. All observed events are sorted and plotted versus their square displacement, r^2 . Then, this curve is fitted (see solid line) to obtain the mean square displacements $\langle r_i^2 \rangle$ for the time interval of 12 s. For more details about the evaluation procedure see text. Panel c shows the mean square displacements obtained by data analysis as depicted in panel b plotted versus time. Squares represent the mobile and dots the stationary fraction. The solid line is a weighted linear plot through the squares. On the basis of eq 2, the slope of this linear fit results in the effective diffusion constant given.

structured M41S-type host. This image was taken with the confocal microscope described in section 2. The bright spots are the diffraction-limited patterns of the emission of individual TDI chromophores, showing the characteristic one-step photobleaching and blinking behavior. The size of the images is $10 \mu\text{m} \times 10 \mu\text{m}$, and the three depicted frames have been taken with a time interval of 4 s. In the first frame (left), the positions of two molecules have been marked with a white circle. The lower one of these two molecules remains stationary and is thus found at the same position in the subsequent frames. The upper molecule diffuses and can therefore be found at different positions at different times. This is visualized in the second and third frames, in which the respective previous positions of the diffusing molecule are indicated by gray circles. This coexistence of approximately 10% stationary and 90% mobile TDI molecules is a general observation made in all samples investigated. An intermediate case of a molecule sticking from time to time is not observed within the temporal (4 s) and spatial (40 nm) resolution of the experiment.

A time series of frames as shown in Figure 2 allows the reconstruction of the trajectories of individual molecules. An exemplary trajectory spanning a total time of 72 s is depicted in Figure 3a. It illustrates that there is no preferential direction for translational motion. This means that the sample is isotropic on the relevant optical scale length used for these experiments, that is, the mesostructure does not exhibit anisotropic structural features above that length scale as indicated by the absence of additional peaks in the X-ray diffractogram. Because the observed trajectories are not unidimensional and because the unidimensional order of the channels is below the optical resolution limit, we use the classical theory for isotropic three-dimensional diffusion to evaluate an effective diffusion constant, D . The microscopic diffusion constant would be obtained for measurements that resolve the channel-like motion. The aforementioned classical theory²⁶ shows that the mean square displacement $\langle r^2 \rangle$ for a particle is proportional to time t :

$$\langle r^2 \rangle = 6Dt \quad (1)$$

Because only the projections of the molecular motions into the focal plane of the confocal microscope are observed, the

evaluation must be performed using the theory for two-dimensional diffusion leading to the relationship²⁶

$$\langle r^2 \rangle = 4Dt \quad (2)$$

To analyze the experimental trajectories in a quantitative manner and to extract the effective diffusion constants, the mean square displacement $\langle r^2 \rangle$ for all diffusion steps observed must be calculated.²⁷ This procedure is exemplified in Figure 3b. Two frames separated by a time interval of 12 s are examined, and the change in position, Δr_i , for each individual molecule is evaluated. This procedure is repeated for all frames separated by this specific time interval. All events observed are ordered, numerated with respect to Δr_i starting with the largest value for Δr_i , and then plotted versus the square of displacement, r^2 . Then, because of the presence of two fractions of differently behaving molecules, this curve is fitted under the assumption of a double Gaussian distribution with the equation

$$N = A_1 \exp(-r^2/\langle r_1^2 \rangle) + A_2 \exp(-r^2/\langle r_2^2 \rangle) \quad (3)$$

rendering two values for the mean square displacements $\langle r_1^2 \rangle$ and $\langle r_2^2 \rangle$ for this specific time interval. The fit through the data (solid line) shows that there is good agreement with this diffusion model. The whole procedure is repeated for all time intervals in a series of frames, and the mean square displacements $\langle r_i^2 \rangle$ obtained are plotted versus time interval (Figure 3c).

To determine the effective diffusion constants of the two fractions from Figure 3c, only the respective data points have been considered. This results in two linear fits according to eq 2 (weighted under consideration of the errors of the basic Gaussian fits) with $D_{\text{mob}} = 3.72 \times 10^{-2} \mu\text{m}^2 \text{s}^{-1}$ and $D_{\text{imm}} = 1.0 \times 10^{-4} \mu\text{m}^2 \text{s}^{-1}$. The value of D_{imm} represents an upper limit for the effective diffusion constant of the stationary fraction of molecules. In our opinion, the value of D_{imm} is due to read-out uncertainties, and this effective diffusion constant therefore only represents an upper limit to a possibly detectable mobility of these molecules. The linear behavior of the mobile fraction clearly shows normal diffusion as the mode of motion.

As is clear from the preparation procedure, the TDI chromophores remain located within micellar aggregates of the sur-

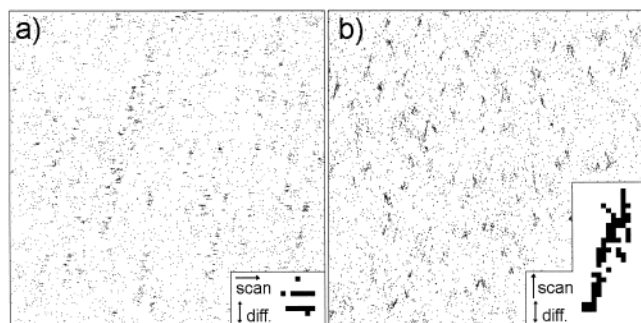


Figure 4. Images taken from TDI diffusing in the lyotropic hexagonal phase of the OMO surfactant and water (1:1). The picture size is $20\ \mu\text{m} \times 20\ \mu\text{m}$. The acquisition time for the whole image is 2 s. The same region was scanned horizontally (panel a; 0°) and vertically (panel b; 87°). The insets show a zoomed-in view of the characteristic patterns generated by the signal from a single molecule.

factants, which served as templates during the synthesis of the mesostructure. Because of their hydrophobic properties, the dye molecules are still located in the inner hydrophobic part of the surfactant micelles in the M41S host. The nearest environment of the dye molecules thus remains unchanged with regard to the surrounding of the molecules in a lyotropic phase built from the surfactant and water.

To put the effective diffusion constant determined above into a meaningful context, we have measured the diffusion of TDI in the hexagonal bulk lyotropic phase consisting of equal parts of OMO and water. It turns out that the translational motion of the chromophores in this phase is much faster than in the molecular sieve. The observation of single-molecule trajectories in the manner described above is not possible on this faster time scale. When scanning a probe with a confocal microscope, two different scan speeds must be considered: The time needed to scan one line determines the time lapse between two adjacent pixels that are situated on two consecutive lines (line-scan speed). The second speed applies for neighboring pixels that lie on the same line (pixel-scan speed). In this case, the time lapse is much smaller. If the diffusion speed of the single molecule comes close to the line-scan speed, it will become relevant in which direction the scan is being performed. For a system with a set of molecules diffusing randomly, no difference in the observed patterns is expected, because nearly the same fraction of molecules is moving along or across the scan direction. Two images of the TDI probe in the liquid-crystalline phase were recorded using quasi-orthogonal scan directions (Figure 4), and a notable difference in the patterns is visible. The pattern observed in the first scan (cf. inset in Figure 4a) is due to the fact that the diffusion transversal to the scan direction is much faster. In this case, the signal from the diffusing molecule will vanish after one or two lines have been scanned. The pattern observed in the second scan is due to the movement of the molecules along the scan direction. In this case, the pattern will span several lines shifting according to the molecule's movement (cf. inset in Figure 4b). A diffusion constant on the order of $1\ \mu\text{m}^2\ \text{s}^{-1}$ was estimated from a movement of 2 pixels (154 nm) in a time interval of $\Delta t = 7.8\ \text{ms}$ between adjacent lines using the one-dimensional diffusion model given in the following equation:

$$\langle r^2 \rangle = 2Dt \quad (4)$$

The obtained information from the images contains directional information. Because in this case our experiment resolves the channel-like motion, we measure a diffusion constant that

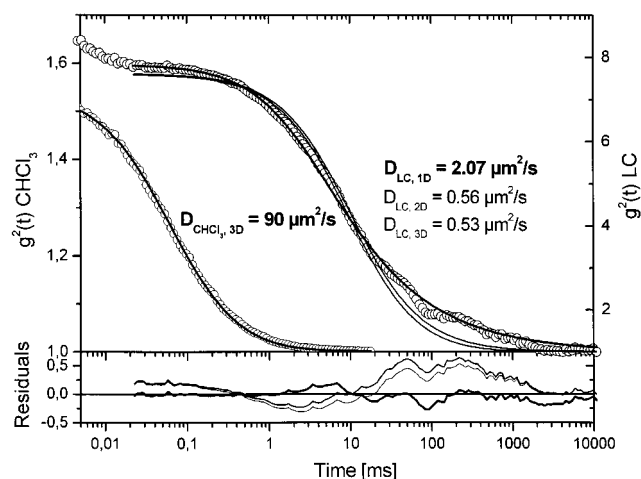


Figure 5. FCS measurement of TDI diffusion in the lyotropic hexagonal phase of the OMO surfactant and water (1:1) and in pure chloroform. The correlation functions were fitted using eqs 5 and 6 for the corresponding diffusion models. Additionally, the curves for the 2D and 3D diffusion models are included (thin lines).

corresponds to the microscopic diffusion constant. The directional information is not available from fluorescence correlation spectroscopy (FCS).²⁸ The fluorescence autocorrelation function for unidimensional diffusion has been derived from Elson et al.²⁸ (see eq 5).

$$G(t) = 1 + A(1 + 4Dt/w^2)^{-1/2} \quad (5)$$

where A is the amplitude, D is the diffusion constant, and $w = 150\ \text{nm}$ is the lateral resolution radius of the used setup. The experimentally obtained autocorrelation curve was fitted using eq 5, yielding a diffusion constant of $D_{\text{LC}} = 2.07\ \mu\text{m}^2\ \text{s}^{-1}$ (Figure 5). The fitting curves for two- and three-dimensional models have been included in Figure 5 to emphasize the difference between the assumed models. To further explain the influence of the micellar structure on the diffusion behavior, the diffusion of TDI in pure CHCl_3 was characterized by FCS (Figure 5) using eq 6 for three-dimensional diffusion.²⁹

$$G(t) = 1 + A(1 + 4Dt/w^2)^{-1}(1 + 4Dt/w_z^2)^{-1/2} \quad (6)$$

where $w_z = 610\ \text{nm}$ is the axial resolution radius of the used setup. Here, the diffusion constant obtained is $D_{\text{CHCl}_3} = 90\ \mu\text{m}^2\ \text{s}^{-1}$. The diffusion constant in solution is therefore significantly larger than that determined in the lyotropic OMO–water structure, which is easily explained by the higher viscosity in the liquid-crystalline phase.

On the experimental scale of length, we can compare the aforementioned diffusion constants with the effective diffusion constant of the TDI molecules after the silica walls have been built around the template. The effective diffusion constant is further reduced by 2 orders of magnitude compared to the diffusion constant in the lyotropic phase.

A combination of two possible effects can explain this behavior. First a further increase of viscosity is likely as the pores shrink during the formation of the silica walls,²⁰ making the surfactant molecules in the micellar template more rigid. An interaction of the molecules with the silica skeleton above the resolution limits of our experiment would show a different form of diffusion. However, because of the high hydrophobicity of the molecules, they are permanently situated within the hydrophobic part of the micelles, ruling out interactions with

the silica framework of the host and explaining the normal diffusion behavior for the mobile fraction of the molecules.

Second, the tortuosity of the channels is likely to be increased because of the formation of the silica walls around them. An increase of the trajectory path due to a higher tortuosity generates a decrease in the observed effective diffusion constant (e.g., a 10-fold increase in path length would generate a 100-fold decrease in the effective diffusion constant, eq 2). The highly isotropic trajectories confirm the presence of tortuous channels.

We cannot, however, discern between the effects of viscosity and tortuosity, because they take place below our temporal and spatial resolution. Another consequence of the transition from an aqueous lyotropic phase to the mesostructure could be that certain micelles become disrupted or blocked. The stationary molecules could be incorporated in such blocked micelles.

4. Summary

The diffusion of single TDI molecules was measured, on one hand, in a micellar environment inside a monolithic silica M41S host and, on the other hand, in the pure hexagonal liquid-crystalline phase of surfactant and water. A large difference in the diffusion behavior is apparent. The one-dimensional anisotropic diffusion paths in the lyotropic phase disappeared after the synthesis of the silica walls indicating the formation of tortuous channels on a length scale below the optical resolution limit. Whereas in the lyotropic phase the channel-like diffusion is observable on the length scale of the optical experiment and thus the microscopic diffusion constant can be obtained, the diffusion in the mesostructured host has to be characterized with an effective diffusion constant, which is 2 orders of magnitude smaller. The reduction in the effective diffusion constant can be attributed to an increase in viscosity and in tortuosity. Apart from the aforementioned mobile fraction, a stationary fraction of ~10% was found. Interestingly, no intermediate case of a molecule sticking from time to time could be observed. The characterization of the effects of geometrical constraints upon the rotational motion of single molecules is currently under investigation. Together these observations will allow a detailed insight into the fundamental processes of molecular diffusion and the interaction between guest molecules and their nearest environment.

Acknowledgment. We thank the DFG for support within the Schwerpunktprogramm "Nanostrukturierte Wirt-Gast-Systeme" and the SFB 486 as well as the VW-Foundation. We also thank G. Jung for helpful discussions.

References and Notes

- (1) Basché, T.; Moerner, W. E.; Orrit, M.; Wild, U. P., Eds. *Single-molecule optical detection, imaging and spectroscopy*; VCH: Weinheim, Germany, 1996.
- (2) Moerner, W. E.; Kador, L. *Phys. Rev. Lett.* **1989**, *62*, 2535.
- (3) Orrit, M.; Bernard, J. *Phys. Rev. Lett.* **1990**, *65*, 2716.
- (4) Basché, T.; Ambrose, W. P.; Moerner, W. E. *J. Opt. Soc. Am.* **1992**, *B9*, 829.
- (5) Eigen, M.; Rigler, R. *Proc. Nat. Acad. Sci. U.S.A.* **1994**, *91*, 5740.
- (6) van Oijen, A. M.; Ketelaars, M.; Köhler, J.; Aartsma, T. J.; Schmidt, J. *J. Phys. Chem. B* **1998**, *102*, 9363.
- (7) Lu, H. P.; Xie, X. S. *Nature* **1997**, *385*, 143.
- (8) Fleury, L.; Dräbenstedt, A.; Gruber, A.; von Borczyskowski, C.; Wrachtrup, J. *J. Phys. Chem. B* **1997**, *101*, 7933.
- (9) Nirmal, M.; Babboussi, B. O.; Bawendi, M. G.; Macklin, J. J.; Trautmann, J. K.; Harris, T. D.; Brus, L. E. *Nature* **1996**, *383*, 802.
- (10) Gruber, A.; Dräbenstedt, A.; Tietz, C.; Fleury, L.; Wrachtrup, J.; von Borczyskowski, C. *Science* **1997**, *276*, 2012.
- (11) Basché, T.; Kummer, S.; Bräuchle, C. *Nature* **1995**, *373*, 132.
- (12) Kulzer, F.; Kummer, S.; Matzke, R.; Bräuchle, C.; Basché, T. *Nature* **1997**, *387*, 688.
- (13) Schmidt, T.; Schütz, G. J.; Baumgartner, W.; Gruber, H. J.; Schindler, H. *J. Phys. Chem.* **1995**, *99*, 17662.
- (14) Dickson, R. M.; Norris, D. J.; Tzeng, Y.-L.; Moerner, W. E. *Science* **1996**, *274*, 966.
- (15) Xu, X.-H.; Yeung, E. S. *Science* **1997**, *275*, 1106.
- (16) Seisenberger, G.; Ried, M. U.; Endress, T.; Büning, H.; Hallek, M.; Bräuchle, C. *Science* **2001**, *294*, 1929.
- (17) Kues, T.; Peters, R.; Kubitschek, U. *Biophys. J.* **2001**, *80*, 2954.
- (18) Bobroff, N. *Rev. Sci. Instrum.* **1986**, *57*, 1152.
- (19) Qian, H.; Sheetz, M. P.; Elson, E. L. *Biophys. J.* **1991**, *60*, 910.
- (20) Attard, G. S.; Glyde, J. C.; Göltner, C. G. *Nature* **1995**, *378*, 366.
- (21) Mais, S.; Tittel, J.; Basché, T.; Bräuchle, C.; Göhde, W.; Fuchs, H.; Müller, G.; Müllen, K. *J. Phys. Chem. A* **1997**, *101*, 8435.
- (22) Kärger, J.; Ruthven, D. M. *Diffusion in Zeolites and Other Microporous Solids*; Wiley: New York, 1992.
- (23) Nijhuis, T. A.; van den Broeke, L. J. P.; van de Graaf, J. M.; Kapteijn, F.; Makkee, M.; Moulijn, J. A. *Chem. Eng. Sci.* **1997**, *52*, 3401.
- (24) Brandani, S.; Ruthven, D. M.; *Chem. Eng. Sci.* **2000**, *55*, 1935.
- (25) Holtrup, F.; Müller, G.; Quante, H.; De Freyter, S.; De Schryver, F. C.; Müllen, K. *Chem.—Eur. J.* **1997**, *3*, 219.
- (26) Berg, H. C. *Random Walks in Biology*; Princeton University Press: Princeton, NJ, 1993.
- (27) Schmidt, T.; Schütz, G. J.; Schindler, H. *Biophys. J.* **1997**, *73*, 1073.
- (28) Elson, E. L.; Magde, D. *Biopolymers* **1974**, *13*, 1.
- (29) Rigler, R.; Mets, U.; Widengren, J.; Kask, P. *Eur. Biophys. J.* **1993**, *22*, 169.